JOURNAL OF Materials CHEMISTRY

# Microemulsion mediated sol–gel synthesis of nano-scaled $MAl_2O_4$ (M = Co, Ni, Cu) spinels from single-source heterobimetallic alkoxide precursors

**Frank Meyer,[a]* Rolf Hempelmann,[a]* Sanjay Mathur[b] and Michael Veith[b]***

[a]*Institute of Physical Chemistry and* [b]*Institute of Inorganic Chemistry, University of Saarland, D–66123 Saarbrücken, Germany. E-mail: veith@rz.uni-sb.de*

***Received 4th January 1999, Accepted 11th May 1999***

Nanocrystalline aluminate spinels with cobalt, nickel or copper as bivalent cations have been prepared in different particle sizes using *single-source* heterometal alkoxides of the type $[M\{Al(OR)_4\}_2]$ ($M^{II}$ = Co, Ni, Cu; R = $Pr^i$, $Bu^t$) in a microemulsion assisted sol–gel process. The compatibility of the metal stoichiometry in the precursor molecules with respect to the spinel requirement was established by elemental, spectroscopic and single crystal X-ray diffraction analyses. Synthesis of $CoAl_2O_4$ using both single- and multi-component routes gave different results: whereas the single-source precursor approach yielded monophasic high purity spinels, phase contamination was evident in the diffractograms of ceramics obtained using a mixture of individual components. The alkoxide precursors were hydrolysed in a homogeneous dispersion of colloidal water droplets in a non-aqueous phase. The diameter of water droplets in the microemulsion can be tuned, *inter alia*, by varying the hydrophilic chain length of the surfactant molecules which influences the size distribution of nanoparticles in the $MAl_2O_4$ ceramics. This parameter is used to obtain nano-spinels with particle sizes in the range 5–45 nm and reveals a qualitative correlation between the initial droplet size and the crystallite size of the resulting spinels. The TG–DTA measurements showed the thermal decomposition to be a three step process with crystallisation of the spinel phase occurring around 900 °C. $^{27}$Al MAS NMR spectra reveal the inverse nature of the obtained spinels. XRD, TEM, SEM, EDX, FTIR and UV–VIS spectral studies were used for characterisation of the powders.

## Introduction

Nanocrystalline ceramics represent an attractive class of materials, which owing to their small size, exhibit novel properties which differ from those of the bulk material. When compared to micro-crystalline ceramics, the different but often desirable behaviour of nano-scaled materials is attributed to the large amount of atoms located in the grain boundaries of the tiny crystallites.[1–4] As a result, nano-structured ceramics display improved properties such as lowered sintering temperatures, increased hardness, stability, diffusion and ductility.[5] However, the synthesis of nano-crystalline materials imposes a challenge on the traditional solid-state synthesis methods which fail to offer a sufficiently narrow size distribution and desired homogeneity at the nanometer level. In this context, the solution methods using alkoxide precursors show promising potential for control over particle size, high purity, good chemical homogeneity, low calcination temperatures and micro-structural uniformity.[6–10] Despite the versatility of alkoxide based sol–gel synthesis, its application is rather limited mainly due to the commercial unavailability of suitable precursors especially for mixed-metal oxides. The sol–gel synthesis of ternary oxides (*e.g.*, pervoskites, $ABO_3$, or spinels, $AB_2O_4$) is usually carried out using a mixture of binary alkoxides as precursors,[11] however, this approach suffers from the different hydrolysis susceptibilities of the individual components and the benefits of improved homogeneity can be lost during the hydrolysis of mixtures of alkoxides which may ultimately lead to component segregation, mixed phases or non-ideal stoichiometry in the final ceramic material.[12] Our efforts in the synthesis of advanced materials are focussed on a single-source precursor approach which involves the use of mixed-metal molecular species with metal ratios compatible to the targeted ceramic material [*e.g.*, $AB_2(OR)_8$ for $AB_2O_4$].[13–17] Using alkoxide precursors in a microemulsion mediated sol–gel process, we have previously reported on a size-controlled synthesis of non-aggregated nanocrystalline pervoskites.[18,19] We describe here the synthesis and characterisation of nano-spinels $MAl_2O_4$ ($M^{II}$ = Co, Ni, Cu). Aluminium based spinels constitute an interesting class of oxide ceramics with important technological applications. Although several chemical routes exist for the preparation of $MgAl_2O_4$ powders,[20–22] the preparation of transition metal–aluminium spinels is limited to fusion of the two component oxides at high temperatures (1000–1600 °C)[23–25] or by co-precipitation reactions in solution.[26,27] Moreover, no literature precedence, to our knowledge, is available on the synthesis and characterisation of nano-scaled transition metal aluminates by a molecular precursor route. The impressive optical (*e.g.*, $CoAl_2O_4$ is well known as Thenard's Blue) and chemical (catalytic applications) properties of transition metal aluminates make them of significant interest as ceramic pigments, coatings, catalysts, *etc.*[27–29] In this contribution, we report the synthesis, influence of synthesis parameters, thermal behaviour and characterisation of nanocrystalline cobalt, nickel and copper aluminates. The results illustrate the effectiveness of the *microemulsion* technique and use of *single-source* precursors in producing nano-ceramics with a narrow size distribution.

## Experimental

The synthesis of heterometal alkoxide precursors was performed using standard vacuum line and modified Schlenk techniques, taking stringent precautions against atmospheric moisture. All hydrocarbon solvents employed in the synthesis of alkoxide and amide precursors were dried using standard procedures[30] and stored over sodium wire or molecular sieves. Isopropyl alcohol was dried by distillation from magnesium turnings and aluminium isopropoxide. Transition metal amides and aluminium alkoxides were synthesised following the published procedures.[31–33] Cobalt carbinolate was obtained by the 1:2 reaction of freshly sublimed $[Co\{N(SiMe_3)_2\}]$ with triphenyl carbinol in toluene. The non-ionic surfactants (Sigma),

constituted of nonylphenol–poly[(*n*) glycol ethers] ($n=7$, 10 or 15), correspond to the so called Tergitols™ TNP-7, TNP-10 and TNP-35 (note: not TNP-15!). The surfactants were of industrial quality and were not purified by HPLC owing to the high cost.

The TG–DTA measurements were performed on a STA 490 analyser (Netzsch, Germany). The precursors were heated in air at a rate of 5 °C min$^{-1}$ in the temperature range 20–1200 °C. The experiments were performed in quartz crucibles which also served as the reference. The sintering of raw powders, obtained after the Soxhlet extraction, was performed in a preheated laboratory tube furnace coupled with a temperature programming device. The IR spectra of spinels were recorded as KBr pellets on a BioRad FTIR–165 spectrometer. The UV–VIS spectra were recorded on a double-beam Perkin-Elmer Lambda 5 photometer. Carbon and hydrogen analyses of the calcined powders were obtained using a LECO CHN900 elemental analyser. Solid-state NMR spectra of polycrystalline samples (*ca.* 200–250 mg) were obtained on a Bruker MSL 200S spectrometer. Powder X-ray diffraction measurements were performed at room temperature on a Siemens D-500 diffractometer operating with Cu-K$\alpha$ radiation. The crystallite size distributions were determined with a computer programme using a modified Warren–Averbach method[34–36] taking in account the line broadening of XRD peak profiles. The powder morphology of the gels before and after heat treatment was investigated using a scanning electron microscope. The recording of SEM micrographs and the energy dispersive X-ray (EDX) analysis were performed, in vacuum, in the specimen chamber of an EDX coupled scanning electron microscope CAM SCAN S4. The TEM images were recorded on a JEM 200 CX transmission electron microscope by drawing a carbon coated copper grid through the suspensions of various ceramics in water.

### X-Ray crystallography

A suitable specimen of $[Co\{Al(OBu^t)_4\}_2]$ was flame-sealed in a Lindemann capillary under an inert atmosphere. Crystal data and structure refinement parameters are given in Table 1. Diffraction data were collected on a Stoe AED 2 diffractometer operating with graphite monochromated Mo-K$\alpha$ X-ray radiation ($\lambda=0.71073$ Å). Unit cell dimensions were determined from the least-squares refinement of $(\sin\theta/\lambda)^2$ values for 25 accurately centered reflections. The intensities were corrected for Lorentz and polarisation factors, and a semi-empirical absorption correction ($\psi$ scans) was applied. The positions of heavy atoms for the structure were determined by direct methods (SHELXS-86)[37a] and the remaining non-hydrogen atoms were located from successive difference Fourier map calculations. The refinements were carried out using full-matrix least squares techniques (SHELXL-97).[37b] All non-hydrogen atoms were refined as individual anisotropic atoms. The hydrogen atoms were added as idealized contributions. The final difference Fourier map was featureless.

Full crystallographic details, excluding structure factors, have been deposited at the Cambridge Crystallographic Data Centre (CCDC). See Information for Authors, 1999, Issue 1. Any request to the CCDC for this material should quote the full literature citation and the reference number 1145/160.

**Table 1** Crystal and structure refinement data for $[Co\{Al(OBu^t)_4\}_2]$

| | |
|---|---|
| Empirical formula | $C_{32}H_{72}Al_2CoO_8$ |
| Formula weight | 697.79 |
| Crystal system | Monoclinic |
| Space group | $P2_1/n$ |
| Unit cell dimensions | |
| $a$/Å | 10.114(2) |
| $b$/Å | 16.578(3) |
| $c$/Å | 25.940(5) |
| $\beta$/° | 93.05(3) |
| $V$/Å$^3$ | 4343.2(14) |
| $Z$ | 4 |
| $\mu$/mm$^{-1}$ | 0.473 |
| $T$/K | 293(2) |
| Reflections collected | 6022 |
| Independent reflections | 6022 |
| Goodness-of-fit on $F^2$ | 1.055 |
| Final $R$ indices [$I>2\sigma(I)$] | $R1=0.0622$, $wR2=0.1524$ |
| $R$ indices (all data) | $R1=0.0922$, $wR2=0.1795$ |

### Synthesis and characterisation of precursors

The heterobimetallic precursors of the general formula $[M\{Al(OR)_4\}_2]$ ($M^{II}$ = Co, Ni, Cu; R = $Pr^i$, $Bu^t$) were prepared by the reaction of anhydrous transition metal halides with potassium tetraalkoxyaluminates as described by Singh and Mehrotra [eqn. (1)].[38,39]

$$MX_2 + 2/n[K\{Al(OR)_4\}]_n \rightarrow [M\{Al(OR)_4\}_2] + 2KX\downarrow \quad (1)$$

(M = Co, Ni, Cu; X = Cl, I)

In an alternative synthetic strategy, the transition metal aluminates were synthesised by the Lewis acid–base interactions of the constituent alkoxides in the parent alcohols. The transition metal alkoxides, $[M(OR)_2]_n$, for this approach were obtained by the alcoholysis of the transition metal silylamides, $[M^{II}\{N(SiMe_3)_2\}_2]$.[31] All the heterometal compounds used in the synthesis of spinels were purified by distillation or sublimation, under reduced pressure. In order to establish the molecular composition of the precursors unambiguously, single-crystal X-ray diffraction analysis was performed on all the *tert*-butoxide derivatives and a representative nickel aluminium isopropoxide. The crystallographic results (Fig. 1) confirm the compatibility of the transition metal : aluminium stoichiometry (1 : 2) with the requirements of $MAl_2O_4$ ceramics. The *tert*-butoxy aluminates of composition $MAl_2(OBu^t)_8$ were found to be isotypical while the nickel aluminium isopropoxide derivative crystallises as an isopropyl alcohol adduct of formulation $[Ni\{Al(OPr^i)_4\}_2]\cdot 2Pr^iOH$. The X-ray crystallography of the Co–Al derivative is discussed here in detail while the structural, spectral and reactivity studies of all other compounds will be published elsewhere.[40]

The molecular structure of $[Co\{Al(OBu^t)_4\}_2]$ (Fig. 1) is based on a spirocyclic metal–oxygen framework. The molecule crystallises in the monoclinic space group $P2_1/n$. It can be conceptually seen as the bidentate interaction of two monoanionic $\{Al(OBu^t)_4\}^-$ moieties with an electrophilic $Co^{2+}$ centre. The three metallic elements show almost linear arrangement (Al–Co–Al 174.5°). The four-membered '$AlO_2Co$' rings are planar (sum of angles 359.57 and 359.86°) and fused at a common center ($Co^{II}$) with their planes being mutually perpendicular. With two terminal ligands present on each of the aluminium atoms, all the metallic elements show four-fold coordination to oxygen. The angular distortions due to the

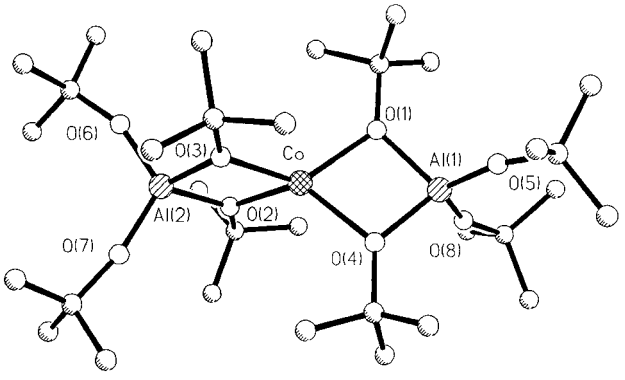


**Fig. 1** Molecular structure of the precursor $[Co\{Al(OBu^t)_4\}_2]$.

constraints of the '$AlO_2Co$' rings are evident in the distorted tetrahedral geometries of all the metal centers, the distortion being more significant for cobalt as revealed in the range of angles around the Co center (77.46–128.30°). The Al–O bond distances can be divided into two types with terminal bond lengths [1.655(4)–1.673(4) Å] being distinctly shorter than bridging Al–O distances [1.800(3)–1.808(3) Å]. The sums of the bond angles at the bridging oxygen atoms approach 360° which indicates these atoms to be $sp^2$ hybridised. The four Co–O distances (Table 2) are essentially similar and reflect the strong chelation of the $\{Al(OBu^t)_4\}^-$ units with the metal centre. These observations indicate the high stability of M–O–Al bridges which support the observation that the mixed-metal alkoxide does not break down into the individual metallic components during hydrolysis reactions. It is relevant to mention that the extraordinary stability of Mg–O–Al bridges in the formation of $MgAl_2O_4$ from $MgAl_2(OR)_8$ has been established by $^{27}Al$ NMR spectroscopic investigations on the partially hydrolysed sols of $MgAl_2(OR)_8$.[41]

### The microemulsion technique

Microemulsions are thermodynamically stable, optically transparent and isotropic systems obtained by the dispersion of water in oil (or oil in water) in the presence of appropriate amounts of surface active reagents. They are widespread in ternary oil recovery, the cosmetic industry and are also used for the synthesis of nanostructured materials, as reviewed recently.[42] Here, we use a water in oil microemulsion system in which tiny water droplets are mesoscopically dispersed in an outer oil phase (reversed micelles) in the presence of nonylphenol poly[(*n*) glycol ethers] as non-ionic surfactants and octan-l-ol as co-surfactant. When dealing with microemulsions, it is extremely important to ensure the position of the system used in its phase diagram.[43,44] In our case, only a single-phase region is desirable, and was confirmed by recording phase diagrams of our microemulsion system.[45]

Sol–gel type synthesis of nano-oxides using microemulsions is based on the principle of controlled hydrolysis of alkoxide precursors in tiny water droplets.[18,19] Since the microemulsions are structured as compartmentalised liquids with water droplets separated into a highly branched and interwoven network of nanometer dimensions, the hydrolysis reactions are confined to the core of individual micelles resulting ideally in monodispersed nano-particles arising from controlled hydrolysis of alkoxide molecules. Earlier investigations on the synthesis of nano-ceramics using the microemulsion technique have shown that the initial droplet size of the micelles, as determined by light scattering experiments, exhibits a governing influence on the resulting crystallite size, possibly due to the limited spatial extension of the droplets, and a correlation between the droplet size and observed crystallite size has been observed.[19,46]

**Table 2** Selected interatomic distances (Å) and bond angles (°) for $[Co\{Al(OBu^t)_4\}_2]$

| | | | |
|---|---|---|---|
| Co–O(3) | 1.964(3) | Al(1)–O(4) | 1.806(3) |
| Co–O(2) | 1.967(3) | Al(1)–O(1) | 1.808(3) |
| Co–O(4) | 1.968(3) | Al(2)–O(7) | 1.655(4) |
| Co–O(1) | 1.973(3) | Al(2)–O(6) | 1.673(4) |
| Co–Al(2) | 2.8504(16) | Al(2)–O(2) | 1.800(3) |
| Co–Al(1) | 2.8504(16) | Al(2)–O(3) | 1.806(3) |
| Al(1)–O(5) | 1.657(4) | Al(1)–O(8) | 1.663(4) |
| O(3)–Co–O(2) | 77.46(12) | O(2)–Al(2)–O(3) | 86.01(14) |
| O(3)–Co–O(4) | 128.01(14) | C(1)–O(1)–Al(1) | 132.1(3) |
| O(2)–Co–O(4) | 125.46(13) | C(1)–O(1)–Co | 130.2(3) |
| O(3)–Co–O(1) | 128.30(12) | Al(1)–O(1)–Co | 97.75(13) |
| O(2)–Co–O(1) | 127.96(13) | C(5)–O(2)–Al(2) | 133.2(3) |
| O(4)–Co–O(1) | 77.60(12) | C(5)–O(2)–Co | 128.5(3) |
| Al(2)–Co–Al(1) | 174.89(5) | Al(2)–O(2)–Co | 98.24(14) |
| O(5)–Al(1)–O(8) | 119.4(3) | C(9)–O(3)–Al(2) | 132.1(3) |
| O(5)–Al(1)–O(4) | 113.5(2) | C(9)–O(3)–Co | 129.7(3) |
| O(8)–Al(1)–O(4) | 109.8(2) | Al(2)–O(3)–Co | 98.15(14) |
| O(5)–Al(1)–O(1) | 111.9(2) | C(13)–O(4)–Al(1) | 132.9(3) |
| O(8)–Al(1)–O(1) | 111.3(2) | C(13)–O(4)–Co | 128.9(3) |
| O(4)–Al(1)–O(1) | 86.23(14) | Al(1)–O(4)–Co | 97.99(14) |
| O(7)–Al(2)–O(6) | 119.0(3) | C(17)–O(5)–Al(1) | 167.3(5) |
| O(7)–Al(2)–O(2) | 111.8(2) | C(21)–O(6)–Al(2) | 159.3(5) |
| O(6)–Al(2)–O(2) | 112.3(2) | C(25)–O(7)–Al(2) | 168.1(6) |
| O(7)–Al(2)–O(3) | 112.5(2) | C(29)–O(8)–Al(1) | 157.6(5) |
| O(6)–Al(2)–O(3) | 110.4(2) | | |

### Synthesis of the spinel ceramics

The essential steps in the synthesis of the ceramics using the microemulsion technique and alkoxide precursors are schematically presented in Scheme 1. The microemulsions were prepared by mixing the oil phase (cyclohexane or *n*-heptane) with Tergitol surfactants and octan-l-ol as co-surfactant. To this system, stoichiometric amounts of water were added with a microsyringe followed by vigorous mixing (2 h) until a translucent emulsion was formed. This microemulsion was added dropwise, under a dry nitrogen atmosphere, to solutions of the respective alkoxides in isopropyl or *tert*-butyl alcohol and stirred for 2 h. The solvents were removed from the amorphous $MAl_2O_4$ dispersions under vacuum and the residue obtained was taken up in acetone to destroy the micelles. The solid product obtained after decantation of the organic phase was dried and Soxhlet extracted (24 h) with cyclohexane to obtain raw precursor powders of spinels which could be transformed to nanocrystalline spinels after calcination at 1000 °C for short time periods.

## Results and discussion

### Comparison between the single-source and multi-component routes

In order to compare the single-source precursor and multi-component approaches, the synthesis of the $CoAl_2O_4$ spinel was performed using both a mixed-metal precursor

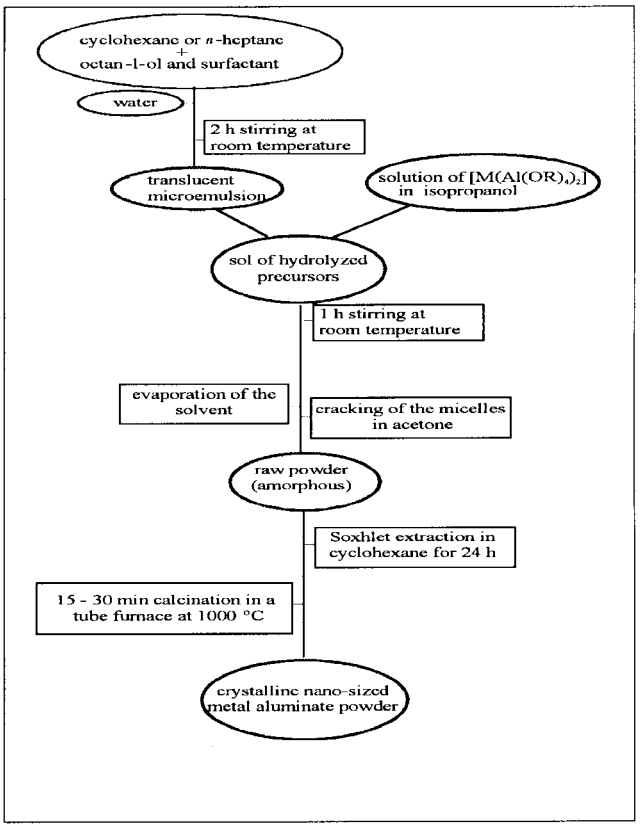


**Scheme 1**

([Co{Al(OBu$^t$)$_4$}$_2$]) and stoichiometric mixtures of component alkoxides {[Al(OPr$^i$)$_3$]$_4$ and Co(OCPh$_3$)$_2$}. We were interested in examining the properties (phase purity, compositional homogeneity, crystallisation temperature, *etc.*) of spinels derived from a molecular precursor containing cross-linked [Co–O(R)–Al] metal centers and the desired metal ratio (Co : Al = 1 : 2) against an alternative and generally practised approach where $Co^{2+}$ and $Al^{3+}$ ions are derived from two individual precursors. Since the simple cobalt alkoxides, [Co(OR)$_2$]$_n$ (R = Et, Pr, Bu$^t$), are insoluble in common organic solvents,[33] they can not be used as starting materials in sol–gel or micro-emulsion methods. In view of the above, soluble cobalt carbinolate was selected as a source for $Co^{2+}$ ions, in the mixed-component approach.

Fig. 2 shows the X-ray diffractogramms of the two differently prepared $CoAl_2O_4$ samples sintered (1000 °C) under similar conditions. It is clearly seen from the powder diffraction patterns that the single precursor synthesis yields much better results in terms of phase purity and crystallinity when compared to the spinel obtained using two separate metal sources, where different hydrolysis kinetics and formation of several species with different metal ratios have to be considered. Since a well defined peak profile is a precondition for a peak shape analysis using the Warren–Averbach method only nanosamples obtained from a single source precursor were suitable for the determination of crystallite size. In view of the above, further investigations on the aluminate spinel systems were restricted to single-source derived powders.

The following section presents the thermal behaviour and characterisation of the amorphous powders and calcined products.

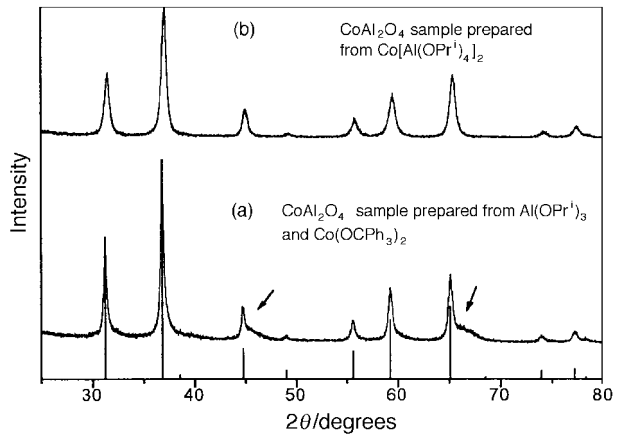


**Fig. 2** X-Ray diffractograms of two $CoAl_2O_4$ samples prepared by (a) multicomponent and (b) single-source precursor routes. Arrows indicate impurities, the vertical lines correspond to the JCPDS indexing.

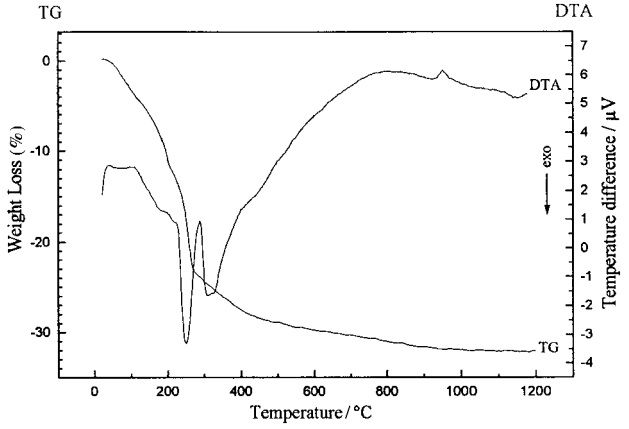


**Fig. 3** TG–DTA profile of the $CoAl_2O_4$ precursor powder obtained using [Co{Al(OBu$^t$)$_4$}$_2$].

## TG–DTA measurements

TG and DTA curves of the thermal degradation of the cobalt aluminate precursor powder are shown in Fig. 3. The total weight loss amounts to 32–34% and occurs in a three step process: (i) initial weight loss resulting from the evaporation of adsorbed alcohol and water; (ii) a second significant weight loss caused by the pyrolysis of the organic compounds (alcohols, acetone, surfactants, co-surfactant, *etc.*) which is observed as two prominent exothermic peaks in the DTA curve; (iii) a third weight loss occurring gradually over a broad range of temperature attributed to pyrolytic elimination of residual hydroxy groups, entrapped gases, *etc.*, as corroborated by a broad endothermic feature between 400 and 800 °C. The crystallisation of $CoAl_2O_4$ spinel is indicated by a broad exothermic feature around 900 °C as no significant weight loss is observed thereafter indicating the formation of an oxide of definite composition. This observation is supported by XRD results which show $CoAl_2O_4$ as the only crystalline phase in the samples heat treated at 900 °C.

## IR spectra

The IR spectra (Fig. 4 and 5) of the raw $MAl_2O_4$ powders (M = Co, Ni or Cu), in all three cases, show metal–oxygen stretching frequencies in the range 500–900 cm$^{-1}$ associated

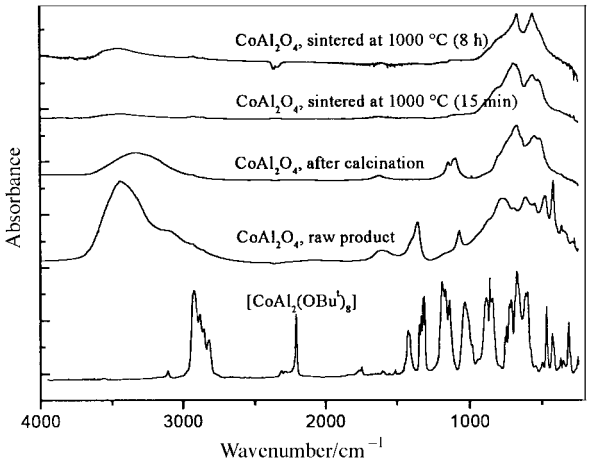


**Fig. 4** IR spectra of raw, calcined and sintered $CoAl_2O_4$ powders obtained using the heterometal alkoxide route.

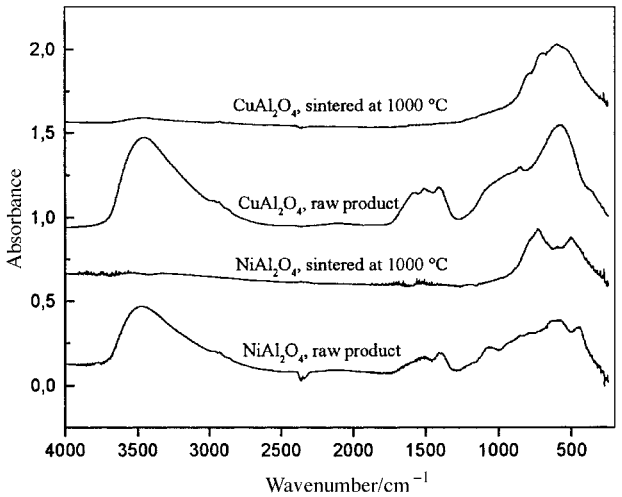


**Fig. 5** IR spectra of the precursor powders and the heat treated (1000 °C) $NiAl_2O_4$ and $CuAl_2O_4$ spinels.

with the vibrations of M–O, Al–O and M–O–Al bonds.[32,47–49] All raw products show broad and intense hydroxy stretching frequencies [$\nu$(OH)] which can be assigned to the overlapping of bands due to surface adsorbed water (*ca.* 3400 $cm^{-1}$) and chemically bonded hydroxy groups (*ca.* 3100 $cm^{-1}$). Residual organic and hydroxy groups evident in raw powders are absent in the calcined samples of $CoAl_2O_4$ and $NiAl_2O_4$ while $CuAl_2O_4$ shows, even after calcination at 1000 °C, residual C–H bands as corroborated by the C and H analyses of the calcined samples (see below). The IR spectra of the molecular precursor [$Co\{Al(OBu^t)_4\}_2$] and $CoAl_2O_4$ powders after various treatments are shown in Fig. 4. In accord with earlier studies,[32] bands in the range 1020–1170 $cm^{-1}$ are assigned to the vibrational modes of the metal attached *tert*-butoxy groups. The asymmetric C–O stretching frequencies due to terminal and bridging $OBu^t$ groups are observed at 910 and 1100 $cm^{-1}$, respectively. The Al–O and Co–O stretching frequencies are found in the range 900–470 and 550–340 $cm^{-1}$, respectively. The characteristic Al–O–Co frequencies (450–800 $cm^{-1}$) present in the molecule are also observed in the raw powder obtained after hydrolysis of the precursor which indicates that the Co–O–Al framework remains intact during the hydrolysis process. The band at 1630 $cm^{-1}$ (Fig. 4) in the raw powders is assigned to the deformation vibration of water molecules [$\delta(H_2O)$]. The intensity of $\nu$(OH) bands decreases on firing the raw material and at 1000 °C the sample contains no hydroxy groups. The appearance of a broad $\nu$(OH) band in the $CoAl_2O_4$ sample (Fig. 4) sintered at 1000 °C is probably due to absorption of water during pelletization with KBr. The absorptions at 1080 and 1160 $cm^{-1}$ in calcined samples correspond to Al–OH bending modes.[50] On comparison with the IR spectral pattern reported[20] for $MgAl_2O_4$ and other substances with spinel-like structures, the two Al–O stretching bands observed in the range 500–900 $cm^{-1}$ can be assigned to different coordination states of Al atoms ($AlO_6$ and $AlO_4$ units). It is probable that the transition metal–oxygen vibrations of the spinels overlap with the Al–O bands. The IR spectra of the raw powders and heat treated samples of $NiAl_2O_4$ and $CuAl_2O_4$ (Fig. 5) are comparable although the bands are broader for $CuAl_2O_4$.

## UV–VIS spectra

Nanocrystalline $CoAl_2O_4$ shows interesting colour changes during heat treatments: the pink raw precursor powder turns olive green upon calcination at 800 °C (crystallite size 8 nm); firing at 1000 °C gives a dark blue ceramic with a particle size of *ca.* 15 nm whilst a characteristic royal blue colour (Thenard's blue) is seen upon heat treatment at 1400 °C (crystallite size >100 nm). It should be noted that the crystalline $CoAl_2O_4$ phase exists at 800 °C as confirmed by XRD and IR studies (see later) and the different samples have the cobalt aluminate composition (EDX analysis). For comparison, we also investigated microcrystalline $CoAl_2O_4$ prepared by the co-precipitation method, but no such colour sequence during sintering was observed. The change in colour with calcination temperature might be an effect of the increasing crystallite size as observed for cadmium sulfide (CdS),[51] however, we have not investigated this phenomenon in detail and the observed colour change might also result from a change in the coordination state of $Co^{2+}$ ion (from octahedral to tetrahedral). The migration of ions from tetrahedral to octahedral sites and *vice versa* (in the case of inverse spinels) during crystallisation is well known for metal aluminates. We have recorded the UV–VIS spectra (Fig. 6) of the amorphous gels and the various crystalline $CoAl_2O_4$ samples sintered at different temperatures. The absorption maxima are in the expected range corresponding to the observed colours. The amorphous sample (pink) does not exhibit a maximum and the absorption was found to decrease steadily with increasing wavelength (Fig. 6).

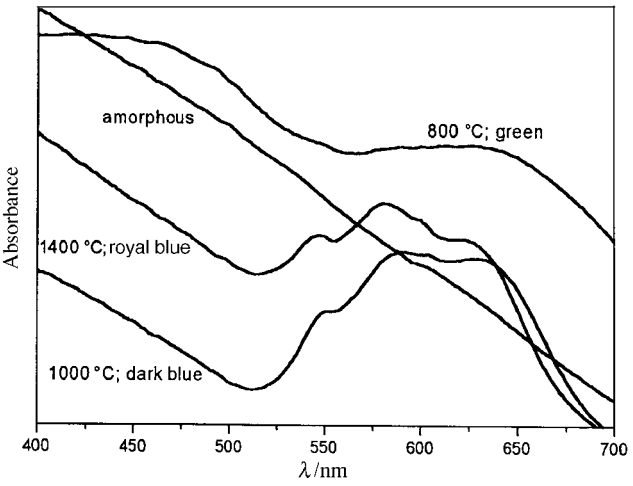


**Fig. 6** UV–VIS spectra of the $CoAl_2O_4$ powders obtained at different stages of heat treatment.

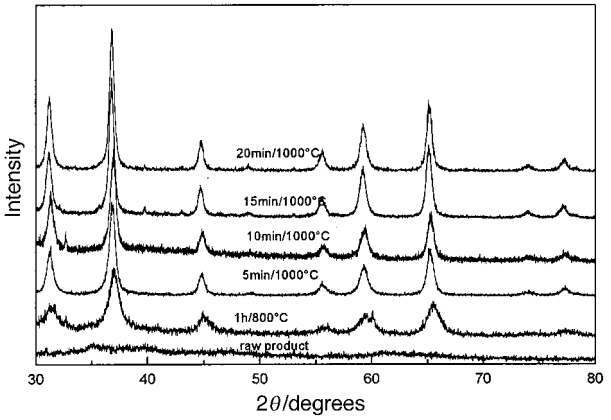


**Fig. 7** Room-temperature X-ray diffractograms of the cobalt aluminate spinel sintered at different temperatures and time periods.

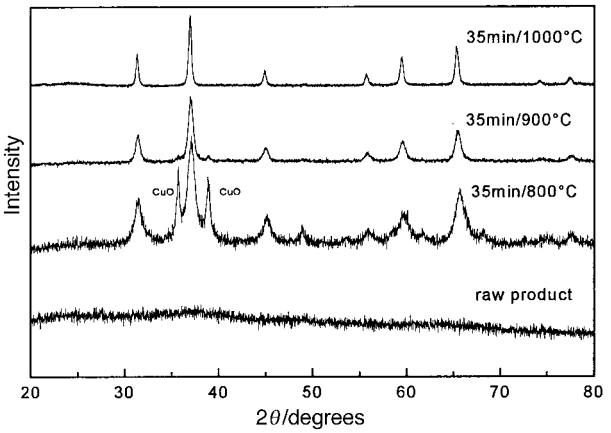


**Fig. 8** Room-temperature X-ray diffractograms of the copper aluminate spinel sintered at different temperatures.

As expected, the absorption maximum of the green sample (800 °C) was found towards longer wavelength whereas the blue samples (1000 and 1400 °C) show broad maxima at lower wavelengths (blue shift). However, no characteristic shift of $\lambda_{max}$ with changing crystallite size was observed.

## Powder X-ray diffraction studies and the effect of calcination temperature

The powder X-ray diffraction patterns of two spinels sintered at different temperatures and times are shown in Fig. 7 and 8.

In order to restrict crystallite growth, the calcination times were carefully monitored to keep them as short as possible. The diffractograms of the samples sintered at 1000 °C indicate that each sample is a monophasic spinel.[52] For cobalt aluminate, substantial crystallinity is achieved at 1000 °C after calcination of the amorphous raw product for 5 min, however, crystallisation proceeds at a much lower temperature and the spinel phase already exists at 800 °C (Fig. 7). Nevertheless, calcination at higher temperature (1000 °C) is necessary for a clean (symmetric) peak profile. In contrast to $CoAl_2O_4$, the raw precursor powder for $CuAl_2O_4$ spinel exhibits a different thermal behaviour. The amorphous raw product does not transform into a pure aluminate phase. Instead an intermediate CuO phase becomes evident at 800 °C which diminishes with increasing temperature and is almost non-existent at 900 °C. This tendency of phase separation has been observed only during the processing of copper aluminate. At 1000 °C, the CuO phase is no longer present and the diffraction pattern reveals monophasic copper aluminate (Fig. 8). Further investigations to understand the formation and conversion of the CuO phase are currently in progress. Fig. 9 shows the corresponding crystallite size distribution of the differently calcined samples and reveals that grain growth occurs with increasing temperature giving rise to broader size distributions. The $NiAl_2O_4$ spinel shows the smallest crystallite size and does not exhibit any unusual thermal behaviour. Nevertheless, obvious crystallite growth with increasing calcination temperature was observed (Fig. 10).

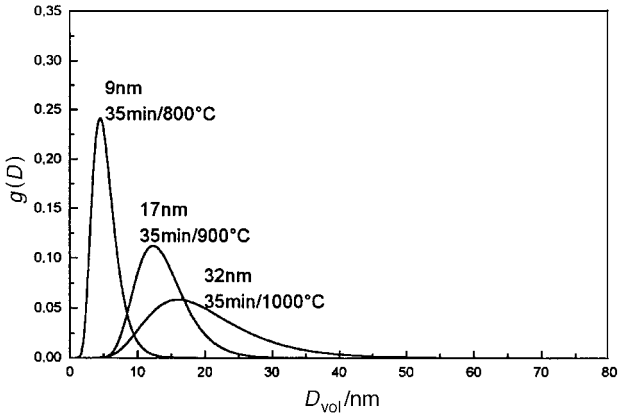


**Fig. 9** Effect of calcination temperatures and time periods on the particle size distribution of the $CuAl_2O_4$ ceramic.

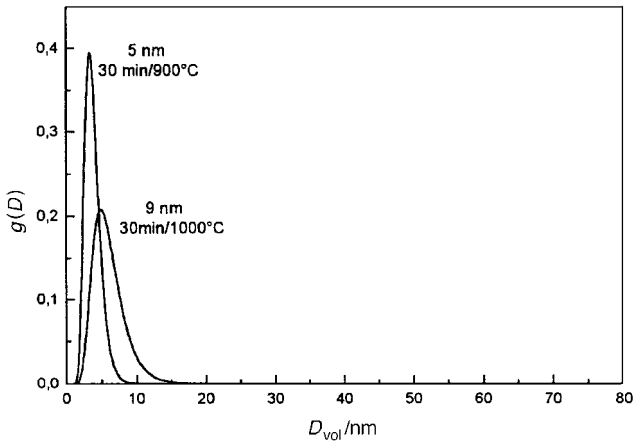


**Fig. 10** Effect of calcination temperatures on the particle size distribution of the $NiAl_2O_4$ ceramic.

### Elemental composition

Energy dispersive X-ray (EDX) analysis performed on several spots for the precursor gels and sintered ceramics shows that there is no detectable variation in the elemental composition at the sub-micrometer level. The elemental compositions determined for all the three systems are within 2% of the intended stoichiometry. The cobalt and nickel aluminate samples after calcination at 1000 °C were found to be free from organic contamination (carbon and hydrogen contents $<0.2\%$) while the copper aluminate sample shows, even at this calcination temperature, a significant amount of carbon (C, 4.9%; H, 3.4%).

### Electron microscopy (SEM/TEM)

Scanning electron micrographs of the raw precursor and heat treated (1000 °C) $CoAl_2O_4$ spinel are shown in Fig. 11. The amorphous raw powder reveals micrometer-sized agglomerated particles with a highly porous structure while the calcined product shows well faceted grains made up of several tiny crystallites. The transmission electron micrographs of the heat treated $CoAl_2O_4$ and $CuAl_2O_4$ samples showed non-agglomerated crystallites whereas agglomerates of nearly spherical particles were observed for $NiAl_2O_4$. A TEM image [Fig. 12(a)] of $CuAl_2O_4$ shows well dispersed particles with crystallite size (30–40 nm) corresponding to the volume averaged values obtained from the peak profile analysis of the XRD results. The crystallinity of the sample is confirmed by the sharp rings

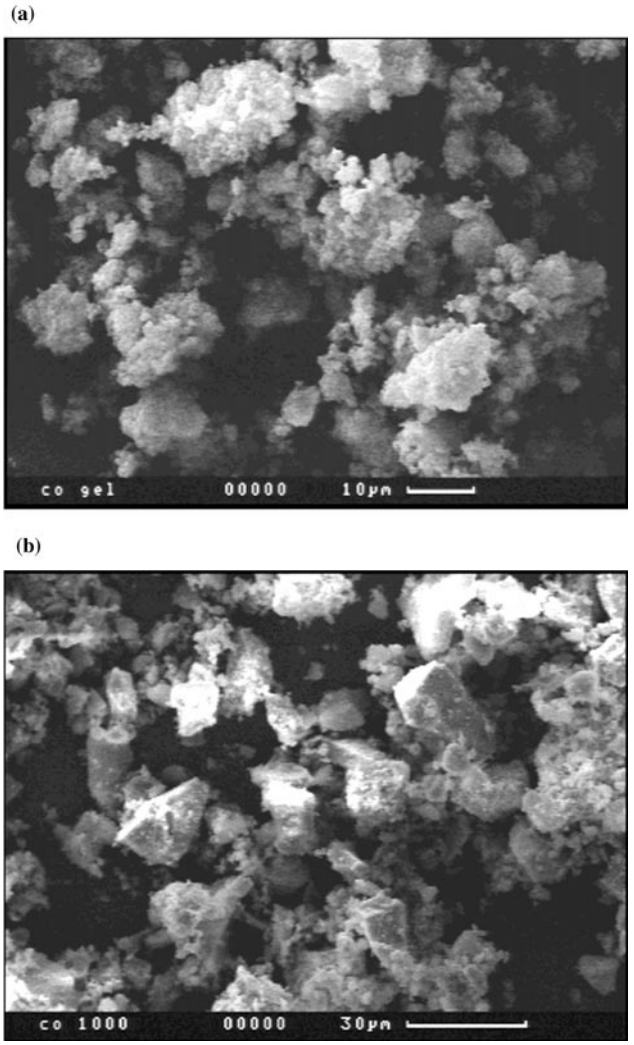


**Fig. 11** SEM micrograph of (a) the raw product obtained in the synthesis of $CoAl_2O_4$ and (b) the spinel after sintering at 1000 °C.

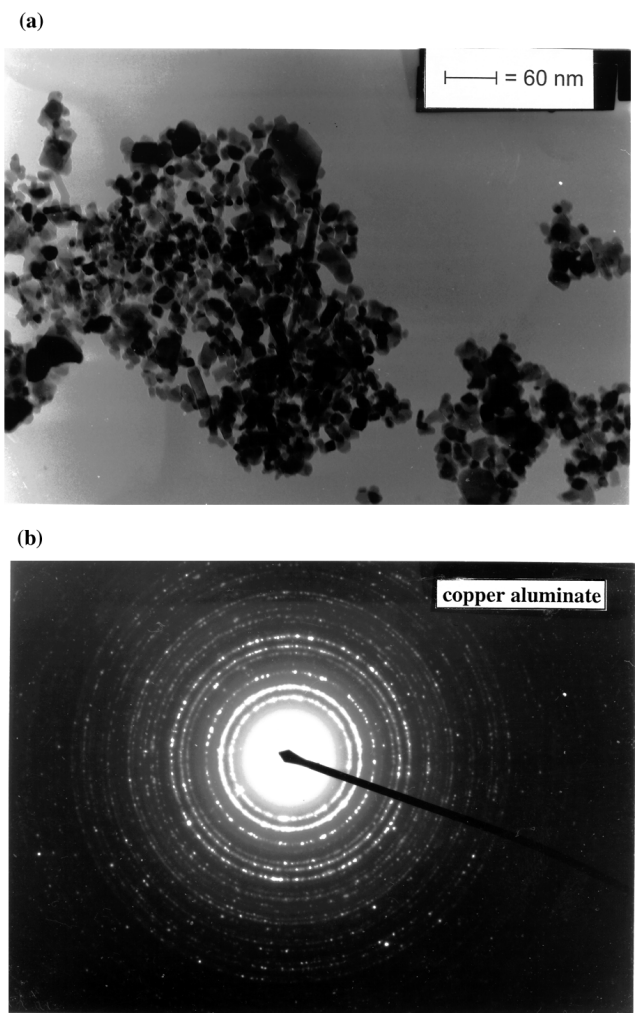


**Fig. 12** (a) TEM micrograph and (b) selected area diffraction pattern of the $CuAl_2O_4$ spinel after sintering at 1000 °C.

observed in the selected area electron diffraction pattern [Fig. 12(b)]. The range of particle size was 15–25 and 10–15 nm for $CoAl_2O_4$ and $NiAl_2O_4$, respectively.

### BET measurements

The specific surface area (Brunauer–Emmett–Teller) of a heat treated (1000 °C) $CoAl_2O_4$ sample calculated from the nitrogen adsorption isotherm is 116.5 $g\,m^{-2}$. The resultant pore-size distribution displays a narrow range of pore diameters with a maximum value of 6.00 nm which matches well with the particle size distribution calculated from the XRD measurements. The heat treated samples of cobalt aluminate could be redispersed in water–isopropyl alcohol in basic media (pH > 12), in the presence of small amounts of colloidal stabiliser (*e.g.*, polyethylene glycol), which is a prerequisite for preparing suspensions for coating glass and other surfaces.

### $^{27}$Al MAS NMR spectroscopy

$^{27}$Al MAS NMR spectroscopy is extremely sensitive in identifying the coordination state of aluminium in aluminium containing materials.[53] In view of the inverse spinel nature of the transition metal aluminates, we thought it worthwhile to examine their $^{27}$Al NMR chemical shifts. The $^{27}$Al MAS NMR spectra of the calcined samples are shown in Fig. 13. For $CoAl_2O_4$, the observed spectrum is broad due to the quadrupolar moment which is much higher for cobalt [$Q(10^{-28}\ m^2)$: $^{59}$Co = 0.42, isotope abundance = 100%] in comparison to nickel [$Q(10^{-28}\ m^2)$: $^{61}$Ni = 0.16, isotope abundance = 1.1%]

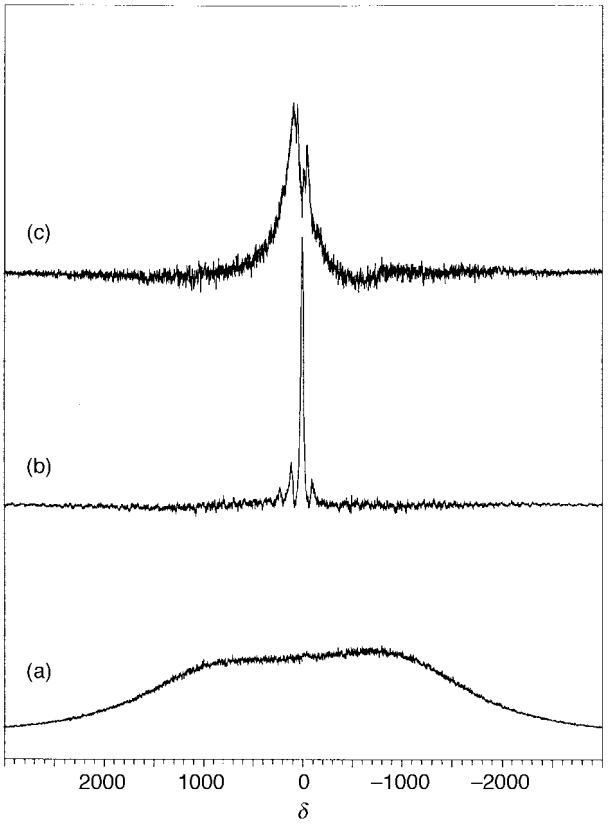


**Fig. 13** The solid-state $^{27}$Al MAS NMR spectra of the nano-spinels sintered at 1000 °C; (a) $CoAl_2O_4$, (b) $NiAl_2O_4$ and (c) $CuAl_2O_4$.

and copper [$Q(10^{-28}\ m^2)$: $^{63}$Cu = −0.22, isotope abundance = 69%; $^{65}$Cu = −0.195, isotope abundance = 30%]. The nickel aluminate spectrum, by contrast, shows a sharp resonance ($\delta$ 3.28) in the region characteristic of six-coordinate aluminium[54,55] suggesting that the paramagnetic influence, among the three divalent ions, on the spectral features is less significant. The spinning side bands in nickel aluminate, spaced at $\approx$80 ppm, are asymmetric in nature indicating a probable overlapping with the signal corresponding to four-coordinate aluminium centers. The $^{27}$Al NMR spectrum of $CuAl_2O_4$ exhibits broad bands in the regions corresponding to tetrahedral and octahedral aluminium sites which indicates an inverse spinel nature with the presence of both $AlO_4$ and $AlO_6$ units in the spinel.

### Influence of the synthesis parameters on the crystallite size of spinels

Previous studies[19,46] have shown that the droplet size in microemulsions can be tuned by variation of nearly all the parameters present in the system. Thus, various factors such as concentration of precursor, water content, water to surfactant ratio and even the temperature at which the system is kept have a significant influence on the crystallite size of resulting ceramics. Tables 3–5 describe the molar compositions of different microemulsions used for hydrolysis of the heterometal compounds and the corresponding average particle sizes determined for the obtained spinels. The crystallite size distributions for various samples are shown in Fig. 14 and 15. The results show that with increasing chain length of the tergitol surfactants a decrease in crystallite size of the cobalt and copper aluminate particles is observed probably due to a corresponding decrease in droplet size (Fig. 14 and 15). For longer hydrophilic chains, fewer molecules are required to stabilise the water droplets; as a consequence, smaller aqueous compartments are formed giving rise to smaller primary particles. Also, the ratio of water to surfactant plays a governing

**Table 3** Effect of the variation of the surfactant chain length (PO = number of polyoxyethylene units) on the resulting crystallite size of $CoAl_2O_4$. The numerical values of the microemulsion constituents correspond to the molar compositions

| Compound | PO units | Water | Surfactant | Octan-l-ol | *n*-Heptane | $D_{vol}$/nm |
|---|---|---|---|---|---|---|
| TNP 35 | 15 | 1 | 0.1 | 0.8 | 12 | 13 |
| TNP 10 | 10 | 1 | 0.1 | 0.8 | 12 | 23 |
| TNP 7 | 7 | 1 | 0.1 | 0.8 | 12 | 25 |

**Table 4** Effect of the variation of the surfactant chain length (PO = number of polyoxyethylene units) on the resulting crystallite size of $CuAl_2O_4$. The numerical values of the microemulsion constituents correspond to the molar compositions

| Compound | PO units | Water | Surfactant | Octan-l-ol | Cyclohexane | $D_{vol}$/nm |
|---|---|---|---|---|---|---|
| TNP 35 | 15 | 1 | 0.1 | 0.28 | 17.5 | 29 |
| TNP 10 | 10 | 1 | 0.1 | 0.28 | 17.5 | 39 |
| TNP 7 | 7 | 1 | 0.1 | 0.28 | 17.5 | 44 |

**Table 5** Effect of the variation of the surfactant concentration on the resulting crystallite size in the synthesis of $CoAl_2O_4$. The numerical values of the microemulsion constituents correspond to the molar compositions

| Compound | Water | Surfactant | Octan-l-ol | *n*-Heptane | $D_{vol}$/nm |
|---|---|---|---|---|---|
| TNP 7 | 1 | 0.11 | 0.24 | 12 | 24 |
| TNP 7 | 1 | 0.14 | 0.24 | 12 | 19 |
| TNP 7 | 1 | 0.25 | 0.24 | 12 | 16 |

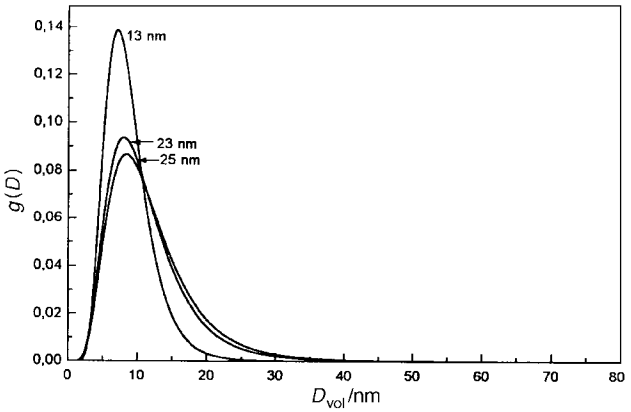


**Fig. 14** Influence on the particle size distribution of cobalt aluminate of varying the chain length of the surfactant molecules.

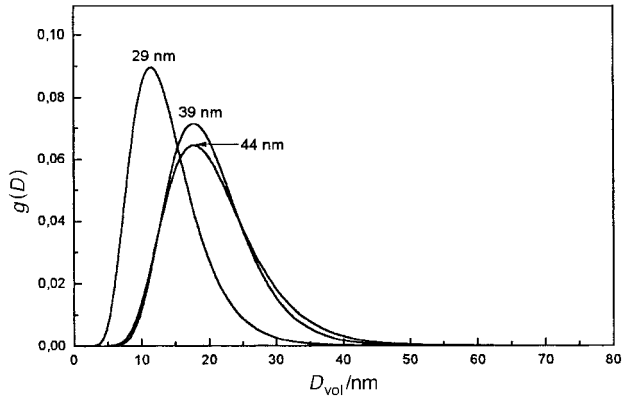


**Fig. 15** Influence on the particle size distribution of copper aluminate of varying the chain length of the surfactant molecules.

role on the size of the water droplets; a lower content of aqueous phase means a smaller equilibrium size of the water droplets within the micelles which ultimately leads to a decrease of the grain size and a narrower particle size distribution in the final ceramic material. Table 5 shows the effect of the surfactant concentration on the resulting crystallite size of cobalt aluminate samples annealed, in each case, for 15 min at 1000 °C. The effect of the variation of the synthesis parameter was found to follow a similar trend in all three cases.

## Conclusion

Nanosized spinels $MAl_2O_4$ (M = Co, Ni, Cu) were prepared by an emulsion templated hydrolysis of alkoxides in the inverse micelles of w/o microemulsions. All the ceramics obtained are monophasic and exhibit well developed spinel phases after remarkably short calcination time periods. The results obtained show the effectiveness of the microemulsion technique for control over the particle size distribution of nano-scaled ceramics. The basic principle of our approach is to produce a highly uniform dispersion of water droplets in an oil phase and to spatially restrict the hydrolysis of the single-source alkoxide precursors within these 'nano-reactors'. By varying the hydrophilic chain length in the surfactant molecules, the diameter of the water droplets can be tuned within the nanometer range. Subject to the synthesis parameters, the size of the resulting nano-sized spinels show a qualitative correlation to the droplet size. Another prominent feature of the present study is the use of heterobimetallic alkoxides $M[Al(OR)_4]_2$, containing both the metallic elements in the desired ratio for $MAl_2O_4$ ceramics, as *single-source* precursors. For a comparative evaluation of single-source and multicomponent approaches, cobalt aluminate samples were synthesised using both the heterometal alkoxide and a stoichiometric mixture of the component alkoxides. The results obtained reveal that the use of heterometal alkoxides assures homogeniety of the ion distribution at the atomic level and a well defined stoichiometry in the resulting oxides.

## Acknowledgement

The authors gratefully acknowledge the financial support of the Deutsche Forschungsgemeinschaft in the framework of the research programme *Sonderforschungsbereich 277* at the University of Saarland, Saarbruecken. R.H. and M.V. thank the Fonds der Chemischen Industrie for their generous support. S.M. thanks the Alexander von Humboldt Foundation, Germany, for a fellowship. We thank Dr Michael Zimmer for recording the solid-state NMR spectra and M. Schuler for the transmission electron microscopy.

## References

1 H. Gleiter, *Prog. Mater. Sci.*, 1989, **33**, 223.
2 S. Komarneni, *J. Mater. Chem.*, 1992, **2**, 993.
3 R. Dagani, *Chem. Eng. News*, 1992, **23**, 18.
4 H. Gleiter, *Nanostruct. Mater.*, 1995, **6**, 3.
5 *Nanomaterials: Synthesis, Properties and Applications*, ed. A. Edelstein and R. C. Cammarata, Institute of Physics Publishing, Bristol and Philadelphia, 1996.

6 D. Segal, *J. Mater. Chem*., 1997, **7**, 1297.
7 R. C. Mehrotra, *Chemtracts: Org. Chem.*, 1990, **2**, 338.
8 C. D. Chandler, C. Roger and M. J. Hampden-Smith, *Chem. Rev*., 1993, **93**, 1205.
9 L. L. Hench and J. K. West, *Chem. Rev*., 1990, **90**, 33.
10 E. Wu, K. C. Chen and J. D. Mackenzie, in *Better Ceramics Through Chemistry*, ed. C. J. Brinker, D. E. Clark and D. R. Ulrich, North Holland, Amsterdam, 1984.
11 P. P. Phule and S. H. Risbud, *J. Mater. Sci*., 1990, **25**, 1169.
12 F. Babonneau, *Polyhedron*, 1994, **13**, 1123.
13 M. Veith, S. Mathur and C. Mathur, *Polyhedron*, 1998, **17**, 1005.
14 M. Veith and S. Kneip, *J. Mater. Sci. Lett.*, 1994, **13**, 335.
15 M. Veith, S. Faber, R. Hempelman, S. Janssen, J. Prewo and H. Eckerlebe, *J. Mater. Sci.*, 1996, **31**, 2009.
16 F. Meyer, A. Dierstein, C. Beck, J. Wagner, W. Härtl, R. Hempelmann, S. Mathur and M. Veith, *Nanostr. Mater.*, 1998, in press.
17 M. Veith, A. Altherr, N. Lecerf, S. Mathur, K. Valtchev and E. Fritscher, *Nanostr. Mater.*, 1998, in press.
18 H. Herrig and R. Hempelmann, *Mater. Lett.*, 1996, **27**, 287.
19 C. Beck, W. Härtl and R. Hempelmann, *J. Mater. Res*., 1998, **13**, 3174.
20 A. K. Adak, S. K. Saha and P. Pramanik, *J. Mater. Sci. Lett*., 1997, **16**, 234.
21 M. Barj, J. F. Bocquet, K. Chhor and C. Pommier, *J. Mater. Sci*., 1992, **27**, 2187.
22 R. E. Rocheleau, Z. Zhang, J. W. Gilje and J. A. Meese-Marktscheffel, *Chem. Mater*., 1994, **6**, 1615.
23 J. W. Mellor, *Trans. Ceram. Soc*., 1937, **36**, 1.
24 J. A. Hedvall and J. Heuberger, *Z. Anorg. Allg. Chem*., 1921, **116**, 137.
25 R. Rieke and W. Paetsch, *Ber. Dtsch. Keram. Ges.*, 1922, **3**, 14.
26 J. E. Baker, R. Burch and N. Yugin, *Appl. Catal.*, 1991, **73**, 135.
27 T. Ohgushi and S. Umeno, *Bull. Chem. Soc. Jpn*., 1987, **60**, 4457.
28 I. A. P. S. Murthy and C. S. Swamy, *J. Mater. Sci*., 1993, **28**, 1194.
29 A. Bhattacharya and V. W. Chang in *Catalyst Deactivation 1994, Studies in Surface Sciences and Catalysts*, ed. B. Delman and G. F. Froment, Elsevier, 1994, vol. 88.
30 A. I. Vogel, *A Textbook of Quantitative Inorganic Analysis*, Longmans, London, 1978.
31 M. F. Lappert, P. P. Power, A. R. Sanger and R. C. Srivastava, *Metal and Metalloid Amides*, Wiley & Sons, New York, 1980.
32 G. A. Sigel, R. A. Bartlett, D. Decker, M. M. Olmstead and P. P. Power, *Inorg. Chem.*, 1987, **26**, 1773.
33 D. C. Bradley, R. C. Mehrotra and D. P. Gaur, *Metal Alkoxides*, Academic Press, London, 1978.
34 W. E. Warren and L. E. Averbach, *J. Appl. Phys*., 1950, **21**, 536.
35 W. E. Warren and L. E. Averbach, *J. Appl. Phys*., 1952, **23**, 497.
36 H. Natter, M. Schmelzer, S. Janssen and R. Hempelmann, *Ber. Bunsen-Ges. Phys. Chem*., 1997, **101,** 1706.
37 (*a*) G. M. Sheldrick, SHELXS-86, *Program for Crystal Structure Determination*, University of Göttingen, 1986; (*b*) G. M. Sheldrick, SHELXL-97, *Program for Crystal Structure Determination*, University of Göttingen, 1997.
38 J. V. Singh and R. C. Mehrotra, *Can. J. Chem*., 1984, **62**, 1003.
39 J. V. Singh and R. C. Mehrotra, *Z. Anorg. Allg. Chem.,* 1984, **512**, 221.
40 M. Veith, S. Mathur, K. Valtchev and V. Huch, manuscript in preparation.
41 K. Jones, T. J. Davies, H. G. Emblem and P. Parks, in *Better Ceramics Through Chemistry*, ed. C. J. Brinker, D. E. Clark and D. R. Ulrich, Pittsburgh, PA, USA, 1986, vol. 73, p. 111.
42 V. Chhabra, M. L. Free, P. K. Kang, S. E. Truesdail and D. O. Shah, *4th International Worlds Surfactants Congress, Special Publication: Economic Outlook, Raw Materials, Synthesis and Characterisation*, 1996, vol. 1, p. 67.
43 M. J. Schwuger, K. Stickdorn and R. Schomäcker, *Chem. Rev*., 1995, **95**, 84.
44 K. V. Schubert and E. W. Kaler, *Ber. Bunsen-Ges. Phys. Chem.* 1996, **100**, 190.
45 A. Dierstein, F. Meyer, M. Quinten, R.Winter, R. Hempelmann, M. Lade and R. Schomäcker, to be published.
46 J. Rivas, M. A. Lopez- Quintela, L. Liz and R. J. Duro, *IEEE Trans. Magn.*, 1993, **29**(6), 26.
47 R. W. Adams, R. L. Martin and G. Winter, *Aust. J. Chem*., 1970, **20**, 773.
48 A. K. Kruger and G. Winter, *Aust. J. Chem.*, 1970, **23**, 1.
49 C. G. Barraclough, D. C. Bradley, J. Lewis and I. M. Thomas, *J. Chem. Soc.*, 1961, 2601.
50 V. Saraswati, G. V. N. Rao and G. V. Rama Rao, *J. Mater. Sci*., 1987, **22**, 2529.
51 A. Henglein, *Ber. Bunsen-Ges. Phys. Chem*., 1997, **11**, 1562.
52 JCPDS Powder Diffraction Data base, File Card Nos. [5–626], [31–174] and [6–399], *Joint Committee for Powder Diffraction Standards*, Swarthmore, 1990.
53 T. Assih, A. Ayral, M. Abenoza and J. Phalippou, *J. Mater. Sci*., 1988, **23**, 3326.
54 M. Kanzaki, *J. Ceram. Soc. Jpn*., 1996, **105**, 98.
55 M. Veith, A. Altherr and H. Wolfanger, *Adv. Mater.*, 1999, **5**, 87.


*Paper 9/00014C*